

Gigahertz Dielectric Polarization of Substitutional Single Niobium Atoms in Defective Graphitic Layers

Xuefeng Zhang,^{1,2,*} Junjie Guo,^{3,6} Pengfei Guan,^{4,‡} Gaowu Qin,^{1,†} and Stephen J. Pennycook^{3,5}

¹Key Laboratory for Anisotropy and Texture of Materials (MOE), School of Materials Science and Engineering, Northeastern University, Shenyang 110819, P. R. China

²National Research Council Canada, 75, de Mortagne, Boucherville, Québec J4B 6Y4, Canada

³Materials Science and Technology Division, Oak Ridge National Laboratory, Oak Ridge, Tennessee 37831, USA

⁴Beijing Computational Science Research Center, Beijing 100084, China

⁵Department of Materials Science and Engineering, National University of Singapore, Singapore 117576, Singapore

⁶Key Laboratory of Interface Science and Engineering in Advanced Materials of Ministry of Education, Taiyuan University of Technology, Taiyuan 030024, P. R. China

(Received 6 January 2015; revised manuscript received 18 August 2015; published 1 October 2015)

We synthesize two Nb/C composites with an order of magnitude difference in the density of single niobium atoms substituted into defective graphitic layers. The concentration and sites of single Nb atoms are identified using aberration-corrected scanning transmission electron microscopy and density functional theory. Comparing the experimental complex permittivity spectra reveals that a representative dielectric resonance at ~ 16 GHz originates from the intrinsic polarization of single Nb atom sites, which is confirmed by theoretical simulations. The single-atom dielectric resonance represents the physical limit of the electromagnetic response of condensed matter, and thus might open up a new avenue for designing electromagnetic wave absorption materials. Single-atom resonance also has important implications in understanding the correlation between the macroscopic dielectric behaviors and the atomic-scale structural origin.

DOI: 10.1103/PhysRevLett.115.147601

PACS numbers: 77.22.-d, 61.48.-c, 81.05.ue

In solids, dielectric phenomena are induced by vibration processes of asymmetric electric charges or dipoles, arising from the polarization of structural heterogeneities polarized in an external electromagnetic field [1,2]. A full understanding of the atomic-scale structural origin of these dipoles is extremely important; however, it is limited by experimental inaccessibility. The broader question, namely, how individual structural sites interact with an electromagnetic field, could provide new insight into the fundamental physics of solid dielectrics and lead to the development of high-performance dielectric materials for technological applications.

Carbon allotropes and their derivatives can be endowed with multiple dipolar configurations at the atomic scale by incorporating vacancies and heteroatoms into the graphitic layers [3–6]. Among these findings, transition-metal atoms at doping sites have been proven to produce considerable changes in the local electronic structure and result in significant physical phenomena including spintronics, plasmonics, magnetism, and dielectrics. Using *ab initio* calculations in a hybrid Co/carbon nanotube structure, Yang *et al.* found an enhanced magnetic moment and spin polarization at the Fermi level [7]. Costa *et al.* [8] and Kirwan *et al.* [9] confirmed theoretically various types of magnetic exchange coupling between metal atoms and carbon nanotubes, demonstrating that the interaction range depends on the position and nature of the foreign atoms. Using electron energy-loss spectrum imaging technology,

Zhou *et al.* observed plasmon resonances of a single silicon atom substituted in a graphene layer, induced by collective oscillations of the electron density at C/Si interfaces, where the individual silicon atom acts as an antenna in the petahertz (10^{15} Hz) range [6]. Additionally, such atomic-scale substitutions can also result in differences, for example, the enhanced dielectric losses at 8–12 GHz for boron-doped carbon nanotubes [10] and the cryogenic electromagnetic absorption at 9 GHz for potassium- and calcium-doped fullerenes [11,12]. Despite these achievements, the overall understanding of the correlation between macroscopic electromagnetic behaviors and the atomic-scale microstructures, particularly for the single-atom configurations, is still relatively poor.

Very recently, we synthesized a (Nb+NbC)/C composite by a modified arc-discharge method, in which single niobium atoms can be stabilized into defective graphitic layers at high density [13]. Both theoretical and experimental studies showed the most probable atomic configuration and a significant electronic interaction between the single niobium atoms and the surrounding carbon atoms. This development provides a new opportunity to study the intrinsic electromagnetic behaviors of single niobium atoms substituted into graphitic layers. In this work, we experimentally observed a strong dielectric polarization phenomenon at ~ 16 GHz for the single-atom Nb/C complex, pointing to the existence of permanent dipoles induced by atomic-scale charge interactions at the

Nb/C heterogeneity. Together with the nanoscale interfacial polarization arising from the NbC/C interfaces, we observe increased complex permittivity in the (Nb+NbC)/C composite across the whole 2–18 GHz range and enhanced dielectric loss at 11–18 GHz.

A fifth-order aberration-corrected scanning transmission electron microscope (STEM, Nion-UltraSTEM100) operated at an accelerating voltage of 60 kV, coupled with an electron energy-loss spectrometer (EELS, Gatan Enfina spectrometer) was employed to study the microstructure of the (Nb + NbC)/C composite. An accelerating voltage of 60 kV, which is below the knock-on damage threshold of graphene, allows nondestructive structural examination of the single niobium atoms. As observed in Figs. 1(a) and 1(b), the carbon matrix was composed mainly of ultra-small NbC clusters with a mean diameter of ~ 1.6 nm. The high-magnification image in Fig. 1(c) provides clear evidence of high-density single niobium atoms (about 3.4×10^5 niobium/ μm^2) uniformly dispersed in the graphitic layers. An ~ 2 nm NbC cluster encased in graphitic shells is directly identified in a magnified annular dark-field (ADF) image and the corresponding composition visualization (ADF) image and the corresponding composition visualization is given in Figs. 1(d)–1(f).

The real part ϵ' and imaginary part ϵ'' of the (Nb+NbC)/C composite, shown in Fig. 2(a), present an overall decline

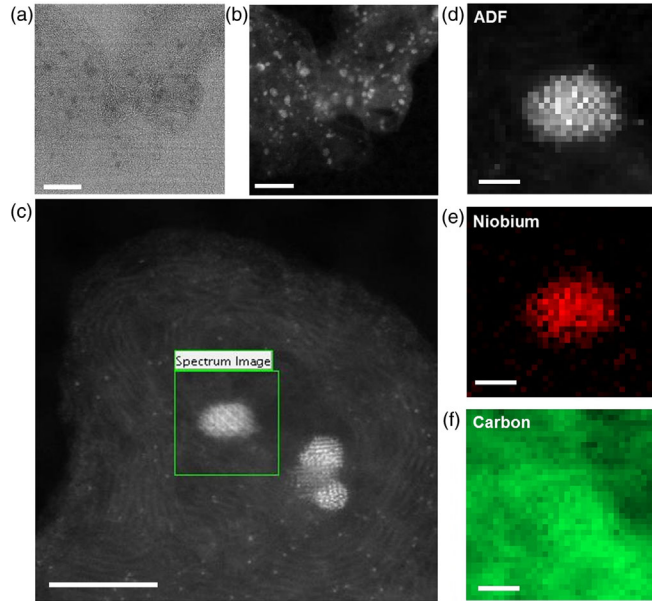


FIG. 1 (color online). Microstructures of a (NbC + Nb)/C nanocomposite consisting of ultras-small niobium carbide clusters and a high density of single niobium atoms in graphitic layers. (a),(b) TEM and STEM images (scale bar: 10 nm). (c) Highly magnified STEM image, showing ~ 2 nm niobium carbide clusters and a high density of single niobium atoms doped into onionlike graphite shells (scale bar: 5 nm). (d)–(f) ADF image of the marked region (green square) in Fig. 1(c) and the corresponding EELs mapping images of niobium and carbon elements (scale bars: 1 nm).

from 66.2 to 25.3 and 31.4 to 15.2, respectively, over the 2–18 GHz frequency range. It should be noted that two obvious resonances appear at ~ 11 and ~ 16 GHz. In comparison, the complex permittivity of the NbC/C composite (Supplemental Material, Fig. S1 [14]) with a much-reduced concentration of single niobium atoms and the larger niobium carbide clusters only exhibits a resonance at ~ 11 GHz [Fig. 2(b)]. Furthermore, the attenuation coefficient α can be calculated from the complex permittivity according to Eq. (1) [15]. As shown in Figs. 2(c) and 2(d), both the dielectric loss factor and attenuation coefficient of the (Nb + NbC)/C composite present two overlapped resonances, while the NbC/C composite only exhibits a resonance behavior at ~ 11 GHz. Here,

$$\alpha = \frac{2\pi f}{c} \left[\frac{(\epsilon'^2 + \epsilon''^2)^{1/2} - \epsilon'}{2} \right]^{1/2}. \quad (1)$$

The dielectric resonance is usually induced by the electron polarization, the ion polarization, and the electric dipolar polarization [16]. At microwave frequencies, the

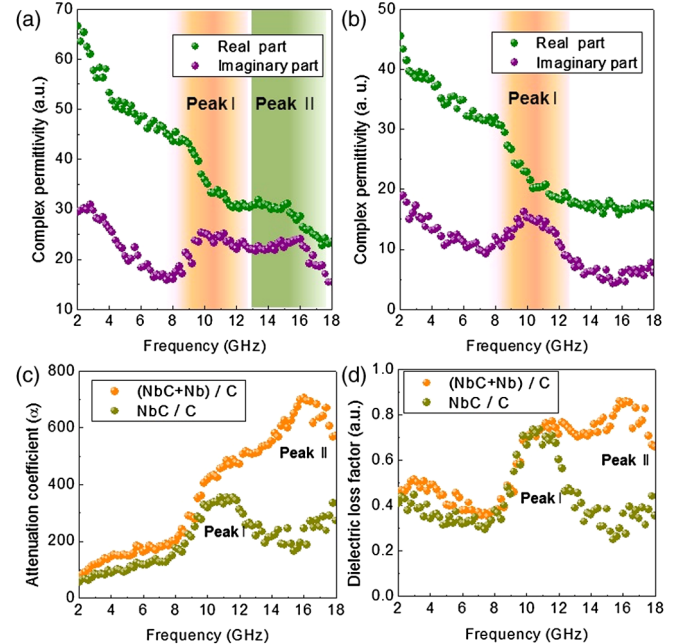


FIG. 2 (color online). Electromagnetic properties of (NbC + Nb)/C and NbC/C nanocomposites. (a),(b) Real part and imaginary part of the complex permittivity of (NbC + Nb)/C and NbC/C nanocomposites as a function of frequency, respectively. (c) Attenuation coefficient plots of (NbC + Nb)/C and NbC/C nanocomposites. (d) Dielectric loss factor plots of (NbC + Nb)/C and NbC/C nanocomposites. In the (NbC + Nb)/C nanocomposite, the attenuation coefficient and dielectric loss factors present two peaks (I and II) at around 11 and 16 GHz, while only one peak appears in the NbC/C nanocomposite. Such a control experiment evidently indicates that the origin of peak II at 16 GHz can be ascribed to the single niobium atoms.

first two polarizations are relatively weak as their dielectric resonances appear at the infrared or higher frequencies. Therefore, the resonances for the (Nb + NbC)/C and NbC/C composites are attributed to the existence of dipolar polarization. Dipolar polarization results from permanent dipoles that arise from the asymmetric charge distribution at heterogeneous interfaces. Under an external electromagnetic field, this polarized charge oscillates at a specific time scale, resulting in a delayed response to the external field (see Fig. S2 and the discussion in the Supplemental Material [14]) [15,17,18].

As to the heterogeneous microstructures, the oscillation of localized space charges at subnanometer scale interfaces is, therefore, considered a main contributor to the dielectric polarization phenomenon with similarities to a boundary layer capacitor [16–22]. Assuming all the NbC clusters are spherical in shape, one can estimate that the increased interface area for the (Nb + NbC)/C composite is about 30% higher relative to the NbC/C composite. The complex permittivity of the (Nb + NbC)/C composite is enhanced by 50% relative to the NbC/C composite across the studied frequency range. Interfacial polarization occurs when the motion of these migrating charges is impeded, and they are trapped within the interfacial region, the so-called Maxwell-Wagner-Sillars polarization [23,24]. Maxwell-Wagner-Sillars polarization usually occurs in the megahertz frequency range, causing a significant variation in

permittivity. If the charge layers are much smaller than the interfacial dimensions, the charge responds independently of the charge on nearby materials (particles). In this case, the charges have time to accumulate at the borders of the materials, resulting in the interfacial polarizations. However, it should be emphasized that, for the NbC/C composite, the particle sizes range from the atomic-scale Nb-C complex to ~ 2 nm NbC clusters, which might be smaller than the charge displacement.

To reveal the origin of the interfacial polarizations, we performed intensive numerical simulations using the finite element solver COMSOL Multiphysics. The calculated permittivity (real parts) for the simulated NbC/C core-shell model [Supplemental Material, Fig. S3(a) [14]] is plotted in Fig. S3(b) [14] and shows the classic dielectric resonance at around 10^{12} Hz for graphitic shell conductivity set to 3×10^3 S/m (the approximate value for the bulk graphite). Clearly, the conductivity of graphitic shells can be seriously degraded due to the high defect density of substitutional niobium or carbon vacancies [25,26], as is seen in microstructural characterizations. By choosing the conductivity of graphitic shells to be 3 S/m, the simulated dielectric resonance frequencies can be adjusted to be $\sim 10^{10}$ Hz, to match our experimental results (~ 11 GHz). Figure S3(c) [14] shows the electric field distributions of the NbC/C nanoparticle for different graphitic shell conductivities at frequencies of 10^8 , 10^{10} , and 10^{12} Hz,

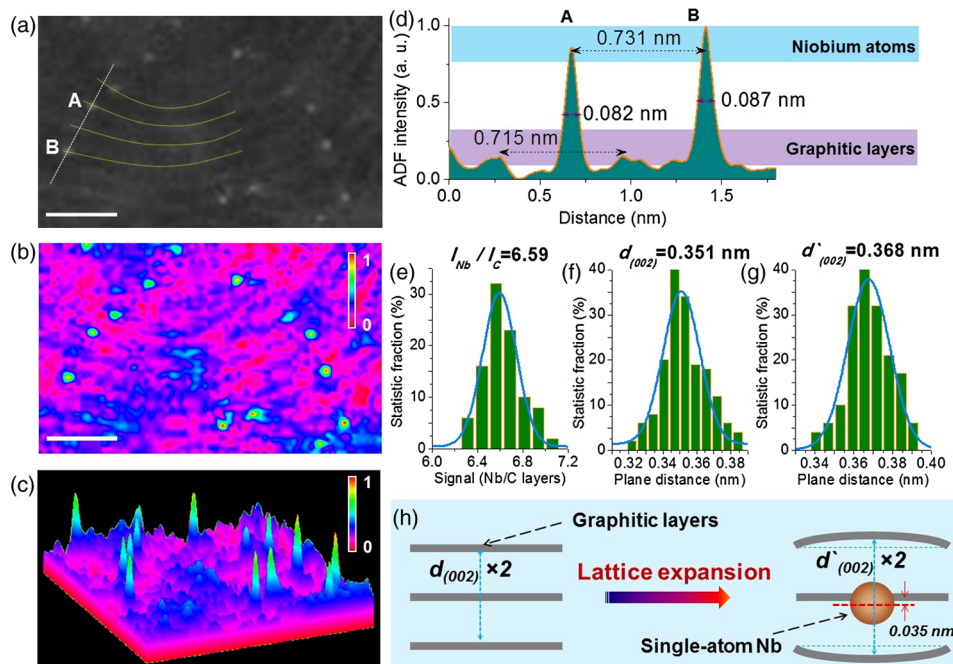


FIG. 3 (color online). Configuration of single niobium atoms in graphitic layers. (a),(b) STEM-ADF Z-contrast images of a high density of single niobium atoms in graphite layers (scale bar: 1 nm). (c) Highly magnified three-dimensional view indicates the ADF intensity of the single niobium atoms and the graphitic layers. (d) ADF intensity profiles of two marked single niobium atoms (A and B) in (a). (e) Statistical ADF intensity ratio of the single niobium atoms to the carbon atoms of graphitic layers from more than 200 measurements. (f)–(g). Statistical (002) plane distances of graphitic layers at two representative regions shown in the left and right panels in (h), respectively.

respectively. At these resonance frequencies, the electric fields rapidly change in the core-shell interfaces, providing the direct view of the interfacial polarizations. Combined with the experimental results and theoretical simulations, the observed resonance at ~ 11 GHz is attributed to the cooperative effect of the core-shell configuration of the NbC/C particles and the degraded conductivity of highly defective graphitic shells.

In addition to the interfacial polarization, the (Nb+NbC)/C composite presents another polarization at ~ 16 GHz. The macroscopic dielectric polarization and loss are ascribed to the existence of permanent dipoles, which could also be achieved by heteroatom doping, for example, K- and Ca-doped fullerenes at cryogenic temperature around ~ 9 GHz [11,12], Li-/Ti-doped oxides at megahertz frequencies [27–29], and nitrogen-doped carbon nanotubes at near-infrared frequencies [30,31]. To understand the formation of a permanent polarization center for single niobium atoms, Fig. 3(a) shows an ADF image focused on a magnified region of single niobium atoms in graphitic layers. Careful observation reveals that these niobium single atoms occupy substitutional sites in carbon atom planes. ADF intensity mapping, associated with atomic numbers, was obtained by using ImageJ digital processing and is shown in Figs. 3(b) and 3(c). Localized ADF enhancement relative to the graphitic layer background appears at the single niobium atom level. The ADF intensity line profile, marked in Fig. 3(a), was evaluated quantitatively in Fig. 3(d). The signal-to-background ratio of ADF intensities for the single niobium atoms to graphitic layers is increased by a factor of 6.64 [Fig. 3(e)]. Furthermore, Figs. 3(f)–3(h) present the average d -spacing distances of the graphitic layers of two representative regions with and without the effect of the single niobium atoms. The mean (002) plane distances are 0.351 and 0.368 nm, respectively, verifying that the substituted niobium atom results in lattice expansion of the graphitic layers [13]. The atomic-scale characterization suggests that the substitutional single niobium atom induces a symmetry breaking in the microstructures and provides a possible explanation for the origin of the electric dipole responsible for dielectric resonance at ~ 16 GHz.

To further explore the single niobium atom polarization, we performed a first-principles calculation using a representative single niobium atom site from the most probable configuration, as shown in Fig. 4(a). The atomic configurations were fully relaxed and the formation energy $\Delta E = E_{\text{Nb+C}} - E_{\text{Nb}} - E_{\text{C-layer}}$ was calculated, in which $E_{\text{Nb+C}}$, $E_{\text{C-layer}}$ and E_{Nb} are the potential energies of a niobium doped graphene (or graphite) layer, a defective graphene (or graphite) layer, and a free niobium atom, respectively. The most energetically favorable configuration is theoretically estimated to be a single niobium atom substituted into a trivacancy site in a carbon atom plane, defined as Nb + G@V₃ (Supplemental Material, Figs. S4–S5 [14]) [13]. In this case, the charge flows from the niobium atom (blue)

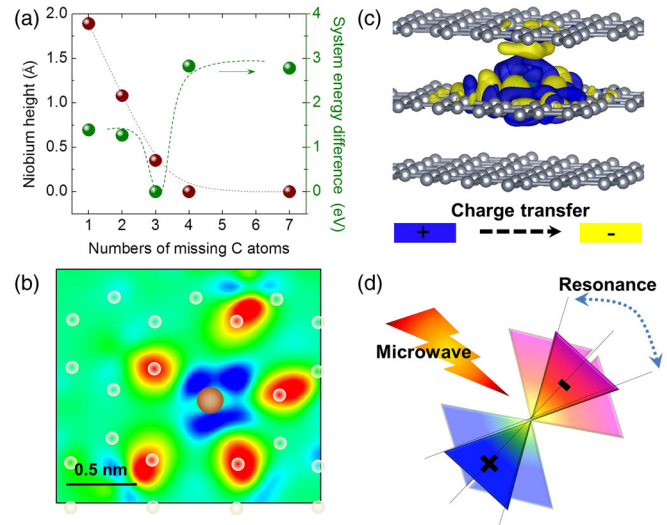


FIG. 4 (color online). Origin of the dielectric polarization of single atom niobium in the (NbC + Nb)/C nanocomposite. (a) Theoretical simulations of possible structure configurations and system energy differences of a single niobium atom incorporated into various defects on a single-layer carbon plane with n missing carbon atoms in a vacancy. (b),(c) Top and side views of the electron density configuration at the vacancy of three missing carbon atoms, showing the asymmetric charge distribution at the region of the single niobium atom site, forming a permanent electric dipole. Charge flows from the niobium atom (blue) into the C atoms (yellow). (d) Schematic of the dielectric resonance of an electric dipole under an external microwave field.

into the C atoms (yellow), as indicated by the top and side-view isosurfaces of the difference in local electron density distributions shown in Figs. 4(b) and 4(c). The consistency between the experimental observations and theoretical predictions strengthens our hypothesis that the single niobium atom substitution gives rise to a local structural asymmetry and results in the formation of a permanent electric dipole that can excite an oscillation under a specific frequency [Fig. 4(d)].

These experimental and theoretical results provide direct evidence for the electromagnetic characteristics of single niobium atoms substituted in graphitic layers at microwave frequencies. The specific electromagnetic resonance indicates that single niobium atoms plays an antennalike role in the microwave-matter interaction process at the excitation energy of $\sim 6.62 \times 10^{-3}$ meV (16 GHz) through the vibration of a permanent dipole arising from symmetry breaking in the localized microstructure. Given the diversity of single metal atoms, a similar phenomenon is likely across various frequencies for doped carbon allotropes and their derivatives. From a fundamental perspective of physics, it would also be significant to explore the electromagnetic characteristics of various substitutional single-atom configurations. Further theoretical and experimental efforts are encouraged to fully uncover these atomic-scale electromagnetic phenomena.

The authors gratefully acknowledge the National Natural Science Foundation of China (Grants No. 51471045 and No. 5152500382), the start-up funding support from the Northeastern University of China, and the Program for Changjiang Scholars, Innovative Research Team in University (IRT0713). This research used facilities provided by Oak Ridge National Laboratory's ShaRE User Facility sponsored by the Scientific User Facilities Division, Office of Basic Energy Sciences, U.S. Department of Energy. P. G. thanks the Center for Computational Materials Science, Institute for Materials Research, Tohoku University, for providing us with the Hitachi SR11000 (Model K2) super-computing system. The authors sincerely appreciate the significant discussion with Dr. Jamal Daoud, Dr. Keith Morton, and Dr. Matthew F. Chisholm.

* zhangxf@atm.neu.edu.cn

† qingw@smm.neu.edu.cn

* pguan@csrc.ac.cn

- [1] S. Brendan, *Principles of Dielectrics* (Oxford University Press, New York, 1998).
- [2] A. K. Jonscher, *Nature (London)* **267**, 673 (1977).
- [3] J. Guo, J. R. Morris, Y. Ihm, C. I. Contescu, N. C. Gallego, G. Duscher, S. J. Pennycook, and M. F. Chisholm, *Small* **8**, 3283 (2012).
- [4] M. F. Chisholm, G. Duscher, and W. Wind, *Nano Lett.* **12**, 4651 (2012).
- [5] O. L. Krivanek, M. F. Chisholm, V. Nicolosi, T. J. Pennycook, G. J. Corbin, N. Dellby, M. F. Murfitt, C. S. Own, Z. S. Szilagy, M. P. Oxley, S. T. Pantelides, and S. J. Pennycook, *Nature (London)* **464**, 571 (2010).
- [6] W. Zhou, J. Lee, J. Nanda, S. T. Pantelides, S. J. Pennycook, and J. C. Idrobo, *Nat. Nanotechnol.* **7**, 161 (2012).
- [7] C. K. Yang, J. J. Zhao, and J. P. Lu, *Phys. Rev. Lett.* **90**, 257203 (2003).
- [8] A. T. Costa, D. F. Kirwan, and M. S. Ferreira, *Phys. Rev. B* **72**, 085402 (2005).
- [9] D. F. Kirwan, C. G. Rocha, A. T. Costa, and M. S. Ferreira, *Phys. Rev. B* **77**, 085432 (2008).
- [10] P. C. P. Watts, W. K. Hsu, A. Barnes, and B. Chambers, *Adv. Mater.* **15**, 600 (2003).
- [11] A. F. Hebard, M. J. Rosseinsky, R. C. Haddon, D. W. Murphy, S. H. M. Glarum, T. T. Palstra, A. P. Ramirez, and A. R. Kortan, *Nature (London)* **350**, 600 (1991).
- [12] A. R. Kortan, N. Kopylov, S. Glarum, E. M. Gyorgy, A. P. Ramirez, R. M. Fleming, F. A. Thiel, and R. C. Haddon, *Nature (London)* **355**, 529 (1992).
- [13] X. F. Zhang, J. J. Guo, P. F. Guan, C. Liu, H. Huang, F. Xue, X. Dong, S. J. Pennycook, and M. F. Chisholm, *Nat. Commun.* **4**, 1924 (2013).
- [14] See Supplemental Material at <http://link.aps.org/supplemental/10.1103/PhysRevLett.115.147601> for the detailed experimental and theoretical methods, the TEM images of NbC@C nanocomposite, the Cole-Cole plots, and the dielectric polarization simulations.
- [15] P. Debye, *Polar Molecules* (The Chemical Catalog, New York, 1929).
- [16] A. Moliton, *Applied Electromagnetism and Materials*. (Springer, New York, 2007).
- [17] S. Tomita, T. Sakurai, H. Ohta, M. Fujii, and S. J. Hayashi, *J. Chem. Phys.* **114**, 7477 (2001).
- [18] A. Mayer, P. Lambin, and R. Langlet, *Appl. Phys. Lett.* **89**, 063117 (2006).
- [19] X. F. Zhang, P. F. Guan, and J. J. Guo, *Part. Part. Syst. Charact.* **30**, 842 (2013).
- [20] P. F. Guan, X. F. Zhang, and J. J. Guo, *Appl. Phys. Lett.* **101**, 153108 (2012).
- [21] X. F. Zhang, P. F. Guan, and X. L. Dong, *Appl. Phys. Lett.* **96**, 223111 (2010).
- [22] C. Wang, T. Chen, S. Chang, S. Cheng, and T. Chin, *Adv. Funct. Mater.* **17**, 1979 (2007).
- [23] R. W. Sillar, *J. Inst. Elect. Eng.* **80**, 378 (1937).
- [24] K. W. Wagner, *Archiv fur Elektrotechnik (Berlin)* **2**, 371 (1914).
- [25] D. Li, W. F. Li, and Z. D. Zhang, *Phys. Rev. B* **73**, 193402 (2006).
- [26] P. M. Ostrovsky, I. V. Gornyi, and A. D. Mirlin, *Phys. Rev. B* **74**, 235443 (2006).
- [27] J. B. Wu, C. W. Nan, Y. Lin, and Y. Deng, *Phys. Rev. Lett.* **89**, 217601 (2002).
- [28] Y. Zhu, J. C. Zheng, L. Wu, A. I. Frenkel, J. Hanson, P. Northrup, and W. Ku, *Phys. Rev. Lett.* **99**, 037602 (2007).
- [29] C. C. Homes, T. Vogt, S. M. Shapiro, S. Wakimoto, and A. P. Ramirez, *Science* **293**, 673 (2001).
- [30] M. A. Kanygin, O. V. Sedelnikova, I. P. Asanov, L. G. Bulusheva, A. V. Okotrub, P. P. Kuzhir, A. O. Plyushch, S. A. Maksimenko, K. N. Lapko, A. A. Sokol, O. A. Ivashkevich, and Ph. Lambin, *J. Appl. Phys.* **113**, 144315 (2013).
- [31] D. Jana, C. L. Sun, L. C. Chen, and K. H. Chen, *Prog. Mater. Sci.* **58**, 565 (2013).